

# Groundwater potential assessment in a sedimentary terrain, southwestern Nigeria

Ahzebobor P. Aizebeokhai<sup>1</sup> · Kehinde D. Oyeyemi<sup>1</sup> · Emmanuel S. Joel<sup>1</sup>

Received: 27 August 2015 / Accepted: 26 May 2016  
© Saudi Society for Geosciences 2016

**Abstract** Geoelectrical resistivity techniques are increasingly being applied in addressing a wide range of hydrological, environmental, and geotechnical problems. This is due to their effectiveness in near-surface characterization. In the present study, a suite of vertical electrical soundings (VESs) was integrated with 2D geoelectrical resistivity and time-domain induced polarization (IP) imaging to characterize the near-surface and delineate the underlying aquifer in a sedimentary terrain. The geophysical survey was conducted as part of preliminary studies to evaluate the potential of groundwater resource in Iyana-Iyesi and Canaan Land area of Ota, southwestern Nigeria. A high-yield confined sandy aquifer overlain by a low-yield aquitard was delineated; overlying the aquitard is a very resistive and thick layer that is predominantly composed of kaolinitic swelling clay intercalated with phosphate mineral.

**Keywords** Groundwater investigation · Resistivity and IP imaging · Near-surface geophysics · Subsurface characterization

## Introduction

Geophysical methods have been used for groundwater exploration and aquifer delineation; they are increasingly becoming more relevant in a wide variety of hydrological

and hydrogeological investigations (e.g., Chandra et al. 2008; Massoud et al. 2010; Niwas and Celik 2012; Hubbard et al. 1999, 2001; Rubin and Hubbard 2005; Vereecken et al. 2006). Geophysical methods are generally non-invasive or minimally invasive, fast, and cost effective, and provide information on the spatial distribution of the physical properties of subsurface features. Thus, the spatial distribution and temporal variability of the subsurface hydrological state can be inferred from the resulting geophysical models. Also, estimates of the hydrological and petro-physical parameters that influence flow and transport processes within the subsurface porous media can be made.

Geoelectrical resistivity technique is one of the most commonly used geophysical methods for hydrological investigations. The technique has been widely used in groundwater exploration to determine depth-to-water table, delineate aquifer geometry, assess groundwater quality, and delineate freshwater-saline water interface (e.g., Wilson et al. 2006). Usually, numerical inversion techniques are used to obtain inverse models of the subsurface electrical resistivity distribution from the measured apparent resistivity data set. This is achieved by solving the non-linear and mixed-determined inverse problem whose solution is inherently non-unique and sometimes unstable. Typically, the resolution of the inverse model differs spatially; some regions of the inverse model may be well resolved while others may exhibit artifacts or anomalies that are not representatives of the physical properties of the subsurface features and, therefore, constitute interpretation errors (Day-Lewis et al. 2005; Loke et al. 2013). In particular, the resolution of the inverse models for subsurface electrical resistivity decreases with depth.

Conventional vertical electrical sounding (VES) has been widely used in geoelectrical electrical resistivity applications for hydrologic, engineering, and environmental

✉ Ahzebobor P. Aizebeokhai  
philips.aizebeokhai@covenantuniversity.edu.ng;  
a.p.aizebeokhai@gmail.com

<sup>1</sup> Physics Department, College of Science and Technology, Covenant University, Ota, Nigeria

investigations. However, in areas where the subsurface geology is relatively complex and subtle such that the spatial distribution of the resistivity varies rapidly over short lateral distances, the conventional resistivity sounding is relatively inaccurate and unable to adequately account for the rapid lateral changes in the subsurface resistivity distribution. Despite this inherent limitation of resistivity sounding technique, VES has been very useful in delineating depth-to-bedrocks and water-table/aquifer, aquifer geometry, interface between freshwater, and saline water, as well as in regional geological studies where the one dimensional model of interpretation is approximately true. Two-dimensional (2D) and/or three-dimensional (3D) resistivity models, which provide more accurate models of the subsurface resistivity distribution (Aizebeokhai et al. 2010b; Loke et al. 2013), are alternatives interpretation models. The 2D and/or 3D geoelectrical resistivity surveys are used to construct reliable 2D and/or 3D models of subsurface resistivity distribution; they are particularly useful in hydrological, environmental, and engineering investigations where the geology is usually more complex and subtle (e.g., Aizebeokhai et al. 2010b; Aizebeokhai and Oyeyemi 2014; Amidu and Olayinka 2006; Chambers et al. 2006, 2011; Dahlin et al. 2002; Dahlin and Loke 1998; Rucker et al. 2010).

Often, geoelectrical resistivity technique is unable to discriminate between saturated sandy and clayey formations as both are characterized with low resistivity anomaly. The resistivity technique is often combined with other geophysical methods such as induced polarization (IP) that is capable of distinguishing clay mineralization from sandy formations. In this study, geoelectrical resistivity soundings were integrated with 2D geoelectrical resistivity and time-domain IP imaging to characterize the subsurface and delineate the aquifer layer. The survey was conducted as part of preliminary investigations for assessing the potential of groundwater resource in Iyana-Iyesi and Canaan Land area of Ota, southwestern Nigeria (Figs. 1 and 2). This assessment is required for groundwater resource development planning as well as monitoring.

### Description and geological setting

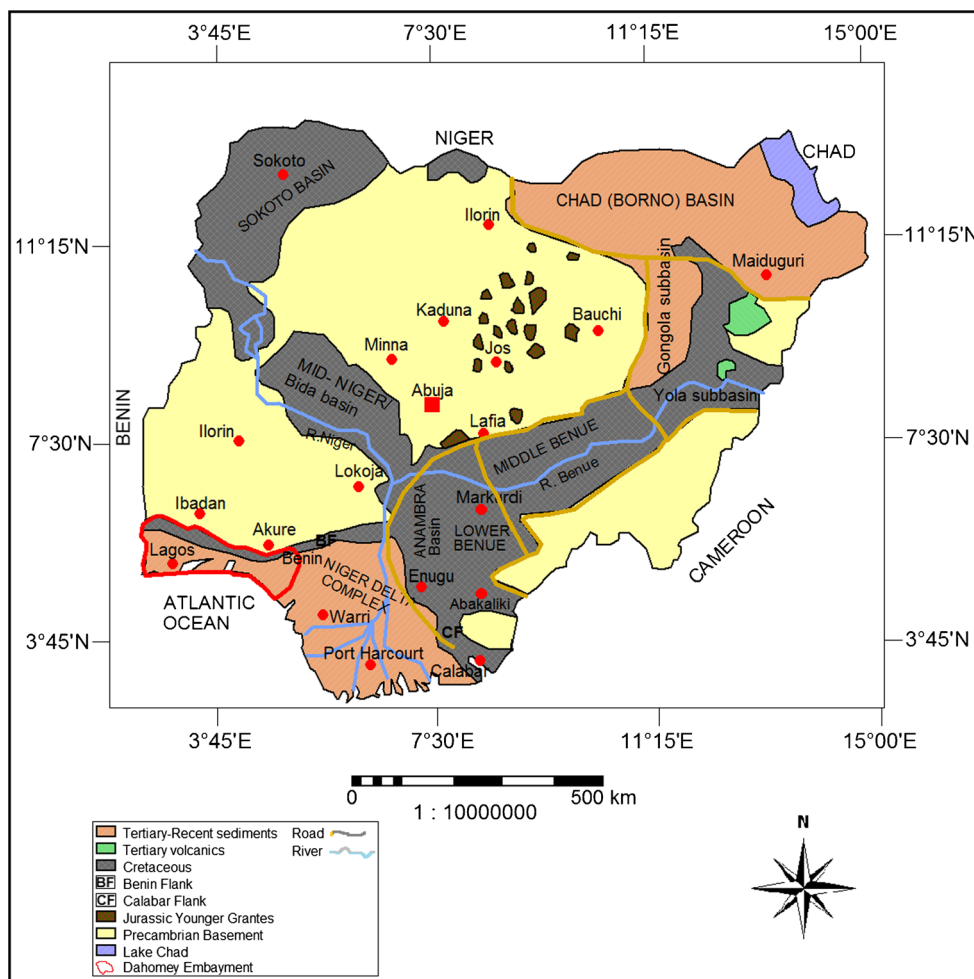
The study area (Figs. 1 and 2) is located in Ado-Odo/Ota Local Government Area of Ogun State, southwestern Nigeria. The topography is gentle sloping with elevation averaging about 75 m above mean sea level; the regional climate is tropical humid characterized by two major climatic seasons—dry and rainy seasons. Usually, the dry season spans from November to early March while the rainy season is between late March and October and is dominated by heavy

rainfall. Occasional rainfall is often witnessed in the area during the dry season because of its proximity to the Atlantic Ocean. Rainfall forms the major source of groundwater recharge in the area as in most tropical humid regions; mean annual rainfall exceeds 2000 mm. The average monthly temperature ranges from a minimum of 23° C in July to a maximum of 32° C in February; mean annual temperature is 27° C.

Geologically, the study area is within the eastern part of Dahomey Basin (Fig. 1); Dahomey Basin is an extensive basin that stretches along the continental margin of the Gulf of Guinea from southern Ghana through Togo and Benin Republic on the west side. The basin is separated from the Niger Delta in the eastern section by the Benin Hinge Line and Okitipupa Ridge; it marks the continental extension of the chain fractured zone (Onuoha 1999; Wilson and Williams 1979). The sedimentary formations of the basin outcrop in an arcuate belt are roughly parallel to the ancient coastline. Sedimentation in the basin was largely controlled by basement fracturing and subsidence associated with the rifting of the South American and African plates. The rocks in the basin are generally Late Cretaceous to Early Tertiary in age (Billman 1992; Ogbé 1970; Okosun 1990; Olabode 2006; Omatsola and Adegoké 1981). The stratigraphy of the basin (Fig. 3) has been grouped into six lithostratigraphic formations. These formations, from the oldest to the youngest, include Abeokuta, Ewekoro, Akinbo, Oshosun, Ilaro, and Benin Formations. However, some of the early researchers described the Cretaceous Abeokuta Formation as Abeokuta Group consisting of Ise, Afowo, and Araromi Formations.

The Cretaceous Abeokuta Formation, which overlies the basement, is predominantly composed of poorly sorted sequence of continental grits and pebbly sands over the entire basin. Occasional siltstones, mudstones, and shale-clay with thin limestone beds due to marine transgression are often observed in the formation. The Abeokuta Formation is overlain by the Ewekoro Formation which is mainly composed of shallow marine limestone due to the contamination of the marine transgression. The limestone-dominated Ewekoro Formation is Palaeocene in age. Overlying the Ewekoro Formation is the shale-dominated Akinbo Formation of Late Palaeocene to Early Eocene (Ogbé 1970; Okosun 1990). The shale and clayey sequence of the Akinbo Formation is concretionary, predominantly kaolinitic and passes gradationally into massive mud/mudstone. The Akinbo Formation is overlain by the Oshosun Formation composed of thickly laminated, glauconitic, and phosphate-bearing Eocene shale with sandstone inter-beds. The Oshosun Formation is overlain by the Ilaro Formation, a predominant sequence of coarse sandy estuarine, deltaic and continental beds with occasional thin bands of phosphate. The Ilaro Formation displays rapid lateral facies changes and is Eocene in age. The Ilaro Formation is overlain by the Benin Formation which is predominantly Coastal Plain Sands and Tertiary alluvium deposits.

**Fig. 1** Geological sketch map of Nigeria showing the major geological components: Basement, Younger Granites, and Sedimentary Basins (modified after Obaje 2009; Aizebeokhai and Oyeyemi 2014)



The local geology of the study area, generally consistent with the regional geology of eastern part of the Dahomey Basin, is predominantly Coastal Plain Sands and Recent sediments. The Coastal Plain Sands consist of poorly sorted clayey sands, reddish mud/mudstone, clay and sand lenses, and sandy clay with lignite of Miocene to Recent. These sediments are underlain by a sequence of coarse sandy estuarine, deltaic, and continental beds of the Ilaro Formation which are largely characterized by rapid changes in facies.

**Geophysical survey**

**Data measurements and field procedure**

The geophysical survey consists of VES and 2D geoelectrical resistivity and time-domain IP imaging. Manual data measurement was adopted; an ABEM Terrameter (SAS 1000 series) was used for the data measurements for both the resistivity soundings and the 2D geoelectrical resistivity and time-domain IP measurements. The survey was designed such that the VESs and traverses cover the entire area of interest;

however, it was largely controlled by accessibility and road network (Fig. 2). The survey was conducted during the months of January and February (dry season), although occasional rainfall was witnessed mainly during the nights. A total of 32 VESs were conducted within the area with the aim of delineating the subsurface layering, depth-to-aquifer, and aquifer geometry. Schlumberger array with maximum half-current electrode separation (AB/2) ranging between 240 and 420 m (but mostly 320 m) was used for data measurements of the resistivity soundings. The number of soundings conducted in the area and electrode spread for each sounding were largely determined by availability of space and accessibility. The electrode spread used for the soundings was considered sufficient for the effective depth of investigation anticipated.

The 2D geoelectrical resistivity and time-domain IP survey was conducted along seven traverses (Fig. 2); Wenner array was used for the data measurements. Each of the traverses was 500 m in length; however, traverse 6 was 450 m long due to space limitation. The electrode separation used for the measurements ranges from 10.0 to 160.0 m in an interval of 10.0 m (10.0 m to 120.0 m electrode spacing was used for

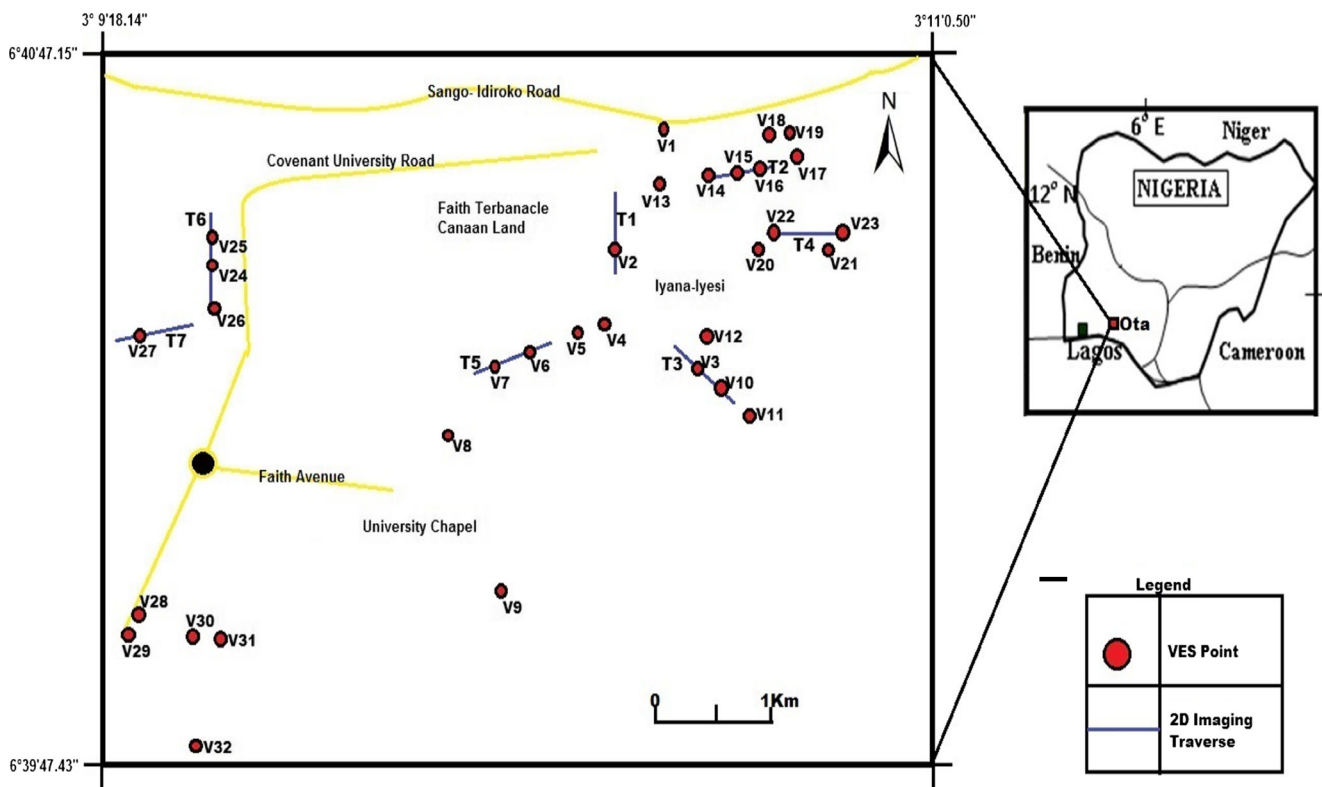


Fig. 2 Map of the study area showing the Traverses and VES location points

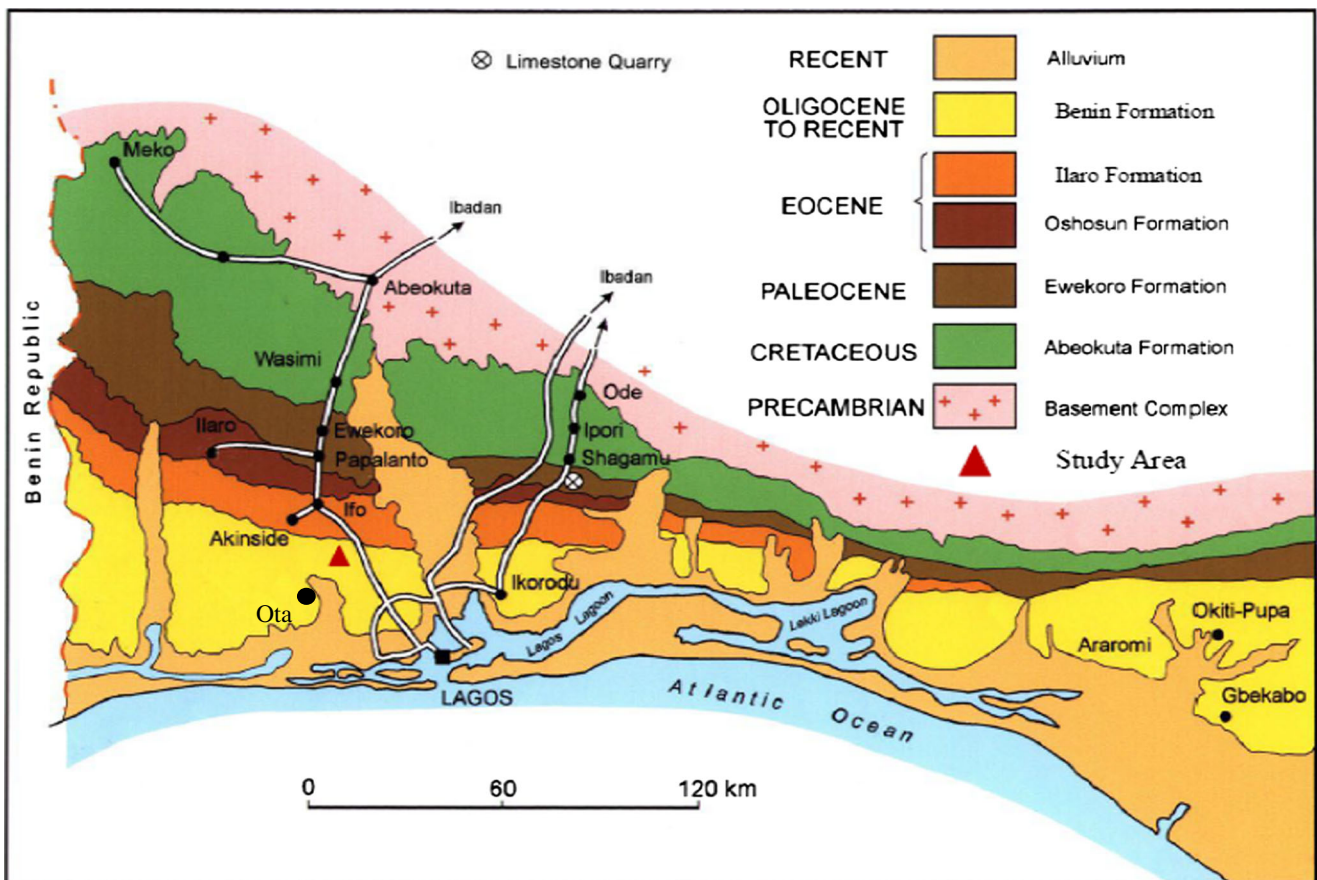


Fig. 3 Geological map of the Nigerian section of Dahomey basin (modified after Gebhardt et al. 2010)

the data measurements in traverses 1, 2, and 6). The 2D apparent resistivity and chargeability (time-domain IP effect) were measured concurrently in all the traverses except for traverses 4 and 5 where only apparent resistivity was measured. The chargeability of the IP effect was measured by integrating the area under the IP decay curve according to the relation

$$M = \frac{1}{V_0} \int_{t_1}^{t_2} V(t) dt, \quad (1)$$

where  $V_0$  is the voltage measured while the current is turned on,  $t_1$  and  $t_2$  is the start and stop time interval, respectively, and  $V(t)$  is the decaying voltage.

To ensure data quality, the electrode positions were clearly marked and pegged before the commencement of the data measurements for each traverse as well as the resistivity soundings. This ensured that electrode positioning error commonly associated with manual multi-electrode data measurements was minimized. The earth resistivity meter was set for repeat measurements with minimum data stacking of 3 and maximum of 6. Good connectivity between the electrodes and the connecting cables was ensured, while maintaining effective contact between the ground and the electrodes. The root-mean-squares error in the measurements was generally less than 0.3 %; however, isolated cases in which the root-mean-squares error was up to 0.5 % were repeated after ensuring the electrodes were maintaining good contact with the ground. The injected current was automatically selected from a minimum of 1.0 mA to a maximum of 200.0 mA by the resistivity meter based on the subsurface conductivity.

### Data processing and inversion

The observed apparent resistivity dataset for the resistivity soundings was plotted against half-current electrode spacing (AB/2) on bi-logarithmic graph sheets. The field curves obtained were then curve-matched with Schlumberger master curves to delineate the number of layers and estimate of the corresponding resistivity and thickness of the delineated layers. The estimated geoelectric parameters were then used as initial models for computer iteration on a Win-Resist program to obtain model geoelectric parameters for the delineated layers.

Similarly, the observed 2D apparent resistivity and chargeability dataset for each traverse were processed and inverted concurrently using RES2DINV inversion code (Loke and Barker 1996). The RES2DINV program uses a non-linear optimization technique that automatically determines the inverse model of the 2D resistivity and chargeability distribution of the subsurface for the measured apparent resistivity and chargeability data set (Griffiths and Barker 1993; Loke and Barker 1996). The RES2DINV program subdivides

the subsurface into a number of rectangular blocks according to the spread and density of the observed data. The size and number of the blocks is determined by the survey parameters (electrode configuration, electrode separations and positions, and data level) used for the data measurements. Least-squares inversion technique with standard least-squares constraint ( $L_2$ -norm or smoothness), which minimizes the square of the difference between the observed and the computed apparent resistivity and chargeability values, was used for the data inversion. The least-squares equation for the inversion was solved using the standard Gauss-Newton optimization technique. Smoothness constraint was applied to both data and model perturbation vectors; appropriate damping factor for the inversion was selected based on the estimated noise level on the measured data.

### Results and discussions

Representative inverse model curves for the geoelectric parameters obtained from the computer iteration of the resistivity soundings are shown in Figs. 4 and 5. The summary of the geoelectric parameters obtained from the inverse model curves are presented in Table 1. In general, nine geoelectric layers were delineated from the sounding curves. The geoelectric parameters of the delineated layers show consistency among the sounding curves, particularly in the deeper sections where the model resistivities and thicknesses are relatively uniform (Table 1). The lithology of the delineated geoelectric layers was established by integrating available information from lithologic samples collected from boreholes and hand-dug wells, known local geology and previous studies (Aizebeokhai et al. 2010a; Aizebeokhai and Oyebanjo 2013; Aizebeokhai and Oyeyemi 2014). The delineated geoelectric layers (from top to bottom) are characterized as top soil, sandy mud/mud stone, sandy/silty clay lens, consolidated lateritic clay, sand lens, lateritic/kaolinitic clay, clayey sand, unconsolidated sand and clay/shale. The geoelectric parameters of some resistivity soundings (selected based on proximity and linearity) were used to construct representative geoelectric cross-sections of the area (Fig. 6).

The top soil is mainly composed of unconsolidated sandy clay and is characterized with low resistivity ranging from 39.7–313.2  $\Omega$ m. The thickness of the top soil varies between 0.5 and 2.3 m. The top soil is underlain by a relatively high resistive layer that is laterally continuous across the study area; this layer is described as sandy mud/sandy mudstone. The inverse model resistivity and thickness of this layer vary largely and ranges from 202.9–1167.6  $\Omega$ m and 0.9–16.6 m, respectively. The large variation observed in the model resistivity of this layer is attributed to differences in the degree of compaction of the unit coupled with lateral changes in

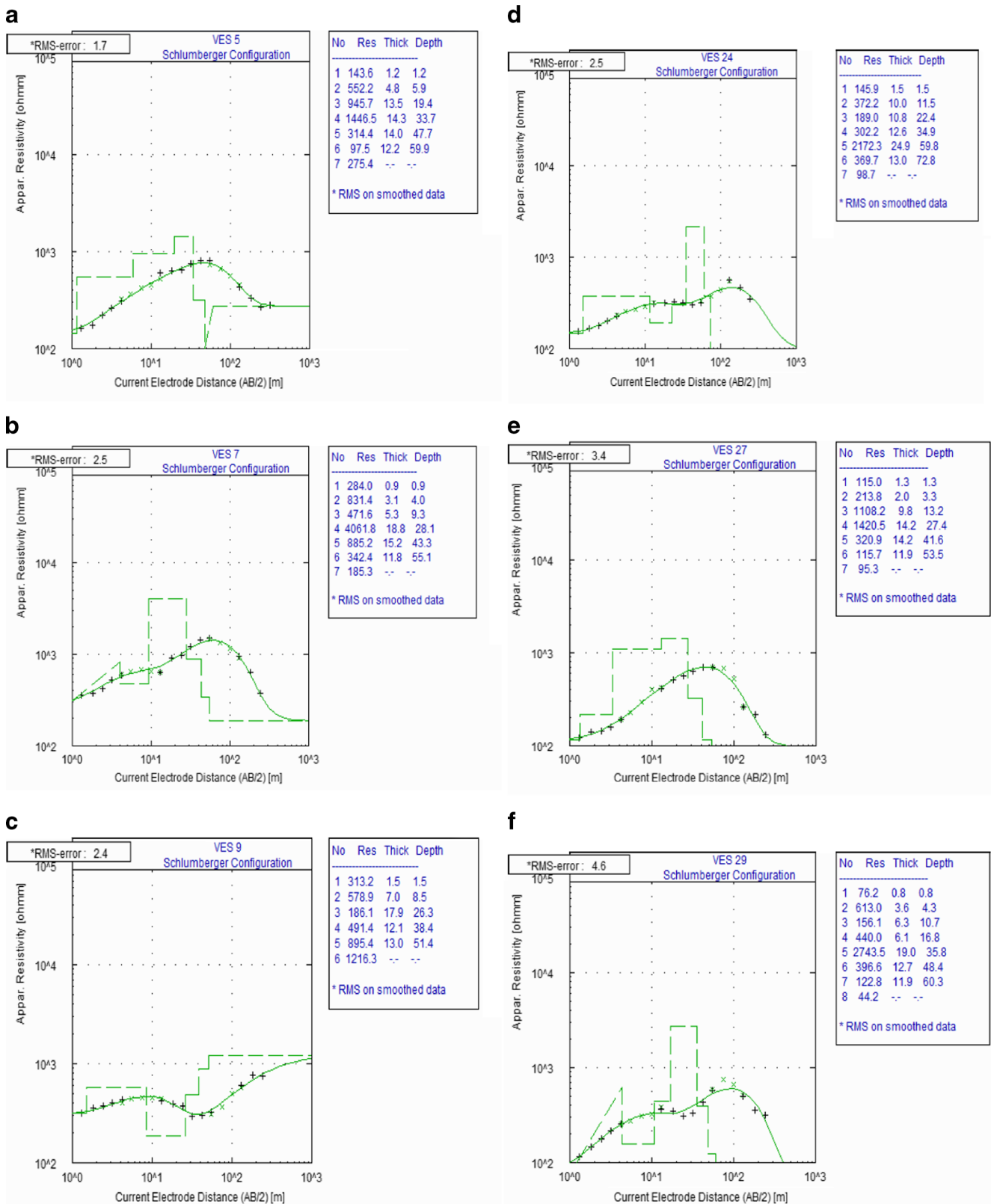


**Fig. 4** Representative vertical electrical sounding curves: **a** VES 5, **b** VES 7, **c** VES 9, **d** VES 24, **e** VES 27, and **f** VES 29

mineralogy. Underlying the second geoelectric layer is a low resistivity sandy/silty clay unit observed to be

laterally discontinuous in the study area; it appears as a lens with varying model resistivity ranging from 56.4

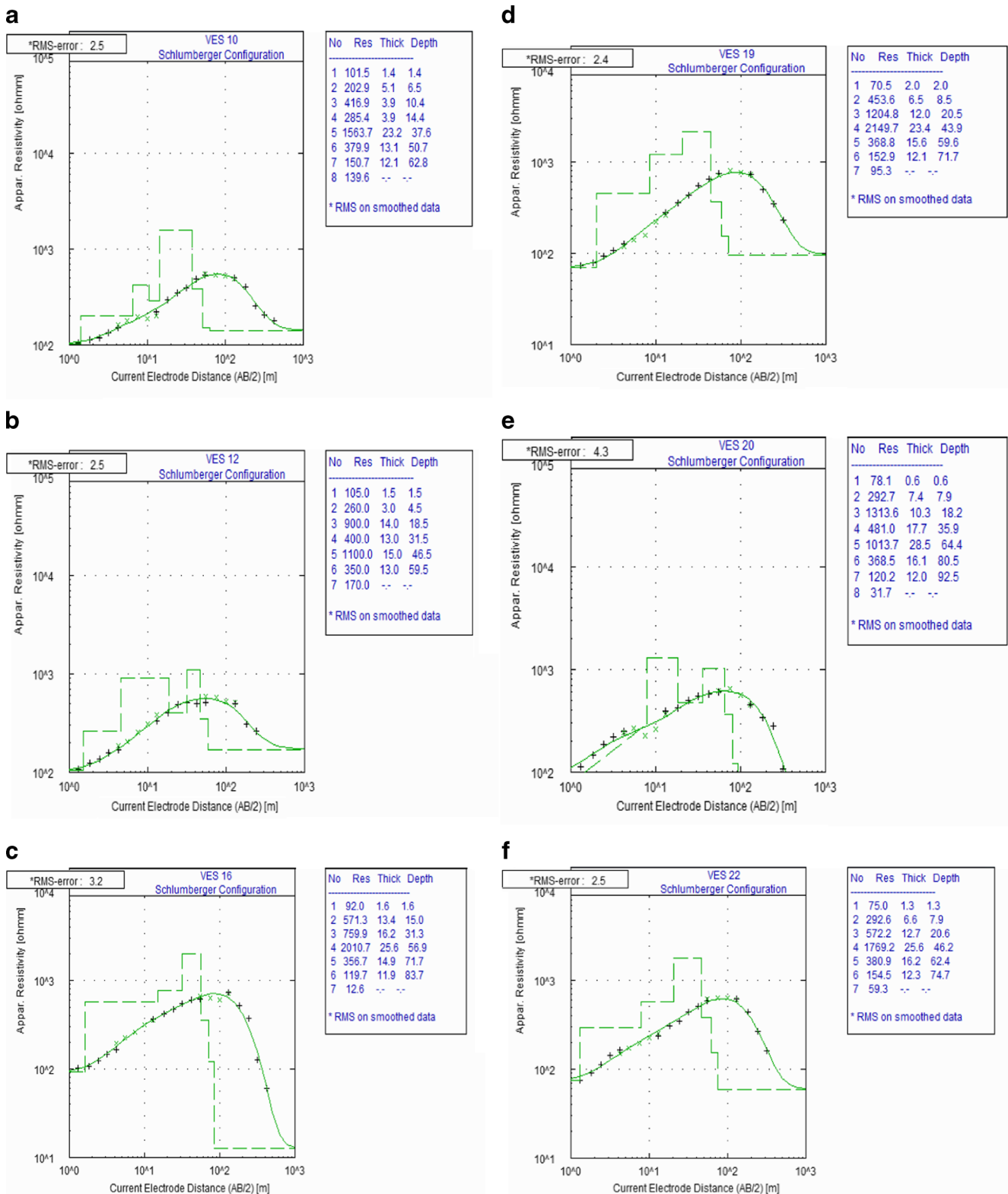


**Fig. 5** Representative vertical electrical sounding curves: **a** VES 10, **b** VES 12, **c** VES 16, **d** VES 19, **e** VES 20, and **f** VES 22

–618.8Ωm and thickness ranging between 2.4 and 22.9 m. The fourth layer delineated is a high resistive unit that is laterally continuous across the study area; it

is underlain by a sand lens in some parts of the study area and merges with the sixth layer in areas where the sand lens is absent.

**Table 1** Geoelectrical parameters obtained from resistivity soundings

Layer	1			2			3			4			5		
	Top soil (sandy clay)			Sandy mud/xandy mudstone			Sandy/silty clay lens			Lateritic clay (compacted)			Sand lens		
	Resistivity ( $\Omega\text{m}$ )	Thickness (m)	Bottom Depth (m)	Resistivity ( $\Omega\text{m}$ )	Thickness (m)	Bottom Depth (m)	Resistivity ( $\Omega\text{m}$ )	Thickness (m)	Bottom Depth (m)	Resistivity ( $\Omega\text{m}$ )	Thickness (m)	Bottom Depth (m)	Resistivity ( $\Omega\text{m}$ )	Thickness (m)	Bottom Depth (m)
VES 4	75.8	1.5	1.5	478.0	3.1	4.6				1286.0	14.0	18.6			
VES 5	143.6	1.2	1.2	552.2	4.8	5.9				945.7	13.5	19.4			
VES 6	172.3	1.1	1.1	849.1	5.8	6.9				1806.4	14.1	21.1			860.2
VES 7	284.0	0.9	0.9	831.4	3.1	4.0		5.3		471.6	18.8	28.1			
VES 8	71.1	0.6	0.6	843.5	1.6	2.2		4.1		133.3	10.8	17.1			
VES 9	313.2	1.5	1.5	578.9	7.0	8.5		17.9		186.1	26.3	38.4			895.4
VES 10	101.5	1.4	1.4	202.9	5.1	6.5		3.9		416.9	10.4	10.4			285.4
VES 11	49.2	1.2	1.2	778.0	2.4	3.6									
VES 12	105.0	1.5	1.5			1.5		3.0		260.0	14.0	18.5			400.0
VES 13	72.0	0.8	0.8	477.7	7.9	8.4		8.4		281.5	9.4	26.6			
VES 14	95.8	1.2	1.2			1.2		7.9		274.7	7.8	16.9			
VES 15	159.0	1.6	1.6	433.3	16.6	18.2									
VES 16	92.0	1.6	1.6	571.3	13.4	15.0				759.9	16.2	31.3			
VES 17	138.7	1.3	1.3	444.1	8.9	10.3				718.9	17.1	27.4			
VES 18	100.8	2.3	2.3	491.8	4.8	7.1									
VES 19	70.5	2.0	2.0	453.6	6.5	8.5									
VES 20	78.1	0.6	0.6	292.7	7.4	8.0									
VES 21	48.4	0.6	0.6	546.0	1.2	1.8		8.0		618.8	11.3	21.2			250.2
VES 22	75.0	1.3	1.3	292.6	6.6	6.6		12.7		572.2	20.6				
VES 23	39.7	1.1	1.1	853.0	6.0	7.1		17.6		547.5	24.6				
VES 24	145.9	1.5	1.5	372.2	10.0	11.5		10.8		189.0	22.3				
VES 25	53.1	0.5	0.5	462.3	1.8	2.3		24.4		121.3	26.7				
VES 26	105.9	0.6	0.6	720.5	3.1	3.7		4.6		125.2	8.3				
VES 27	115.0	1.3	1.3	213.8	2.0	3.3									
VES 28	177.6	0.8	0.8	681.1	6.8	7.6		9.6		368.9	17.2				
VES 29	76.2	0.8	0.8	613.0	3.6	4.4		6.3		156.1	10.7				
VES 30	312.1	1.3	1.3	616.5	10.9	12.2									
VES 31	230.4	0.8	0.8	511.8	4.3	5.1		7.7		60.6	12.8				
VES 32	63.6	0.5	0.5	367.1	0.9	1.4		2.4		56.4	3.8				
Mean	119.0	1.2	1.2												
Layer	5			6			7			8			9		
Lithology	Sand lens			Lateritic/kaolinated clay (confining bed)			Clayey sand (aquitard)			Sand (main aquifer)			Shale /clay		
Location	Thickness (m)	Bottom Depth (m)	Resistivity ( $\Omega\text{m}$ )	Thickness (m)	Bottom Depth (m)	Resistivity ( $\Omega\text{m}$ )	Thickness (m)	Bottom Depth (m)	Resistivity ( $\Omega\text{m}$ )	Thickness (m)	Bottom Depth (m)	Resistivity ( $\Omega\text{m}$ )	Thickness (m)	Bottom Depth (m)	Resistivity ( $\Omega\text{m}$ )
VES 4	18.6	1575.0	14.3	32.9	367.1	13.8	46.7	107.9	12.7	59.4	66.9				
VES 5	19.4	1446.5	14.3	33.7	314.4	14.0	47.7	97.5	12.2	59.9	275.4				



**Table 1** (continued)

Layer	5			6			7			8			9		
	Sand lens			Lateritic/kaolinated clay (confining bed)			Clayey sand (aquitard)			Sand (main aquifer)			Shale /clay		
Location	Thickness (m)	Bottom Depth (m)	Resistivity ( $\Omega$ m)	Thickness (m)	Bottom Depth (m)	Resistivity ( $\Omega$ m)	Thickness (m)	Bottom Depth (m)	Resistivity ( $\Omega$ m)	Thickness (m)	Bottom Depth (m)	Resistivity ( $\Omega$ m)	Thickness (m)	Bottom Depth (m)	Resistivity ( $\Omega$ m)
VES 6	7.7	28.8	2117.5	13.8	42.5	305.9	14.8	57.4	84.0	19.6	77.0	970.1			
VES 7		28.1	885.2	15.2	43.3	342.4	11.8	55.1	185.3						
VES 8		17.1	2255.4	16.9	34.0	346.9	11.9	45.8	63.4						
VES 9	13.0	51.5	1216.3												
VES 10	4.0	14.4	1563.7	23.2	37.6	379.9	13.1	50.7	150.7	12.1	62.8	139.6			
VES 11		3.6	1006.7	38.2	41.8	369.4	12.8	54.6	172.8	12.5	56.8				
VES 12	13.0	31.5	1100.0	15.0	46.5	350.0	13.0	59.5	170.0						
VES 13		26.6	3552.2	18.0	44.6	369.9	11.9	56.5	119.5	11.9	68.4	38.2			
VES 14		16.9	4231.7	23.8	40.7	369.2	11.7	52.4	118.8	11.8	64.1	18.1			
VES 15		18.2	3318.4	21.0	39.2	399.5	13.9	53.1	159.7	13.0	66.1	58.4			
VES 16		31.3	2010.7	25.6	56.9	356.7	14.9	71.7	119.7	11.9	83.7	12.6			
VES 17		27.4	2644.6	27.0	54.4	364.2	15.6	70.0	152.4	12.1	82.1	66.3			
VES 18		7.1	1464.7	34.0	41.1	363.2	15.0	56.1	188.0	13.3	69.4	53.7			
VES 19		20.5	2149.7	23.4	43.9	368.8	15.7	59.6	152.9	12.1	71.7	95.3			
VES 20	17.7	36.0	1013.7	28.5	64.5	368.5	16.1	80.6	120.2	12.0	92.6	31.7			
VES 21	14.6	35.8	1221.1	18.7	54.5	415.3	13.7	68.2	126.8	12.2	80.5	25.6			
VES 22		20.6	1769.2	25.6	46.2	380.9	16.2	62.4	154.5	12.3	74.7	59.3			
VES 23		24.6	1176.9	33.3	57.9	371.0	16.1	74.0	120.2	13.0	87.0	30.9			
VES 24	12.6	34.9	2172.3	24.9	59.8	369.7	13.0	72.8	98.7						
VES 25	12.6	39.3	3191.2	22.2	61.5	356.1	11.9	73.4	73.9						
VES 26	29.2	43.6	2572.0	25.2	68.8	400.2	13.9	82.7	68.1						
VES 27		13.2	1420.5	14.2	27.4	320.9	14.2	41.6	115.7	11.9	53.5	95.3			
VES 28		28.6	770.9	8.9	37.5	305.2	10.9	48.4	106.5	12.2	60.6	50.1			
VES 29	6.1	16.8	2743.5	19.0	35.8	396.6	12.7	48.4	122.8	11.9	60.3	44.2			
VES 30	16.2	41.1	6925.8	41.5	82.5	384.8	13.1	95.6	228.3						
VES 31		21.2	4077.1	29.9	51.1	382.2	12.5	63.6	58.8						
VES 32	23.3	33.4	787.3												
Mean															

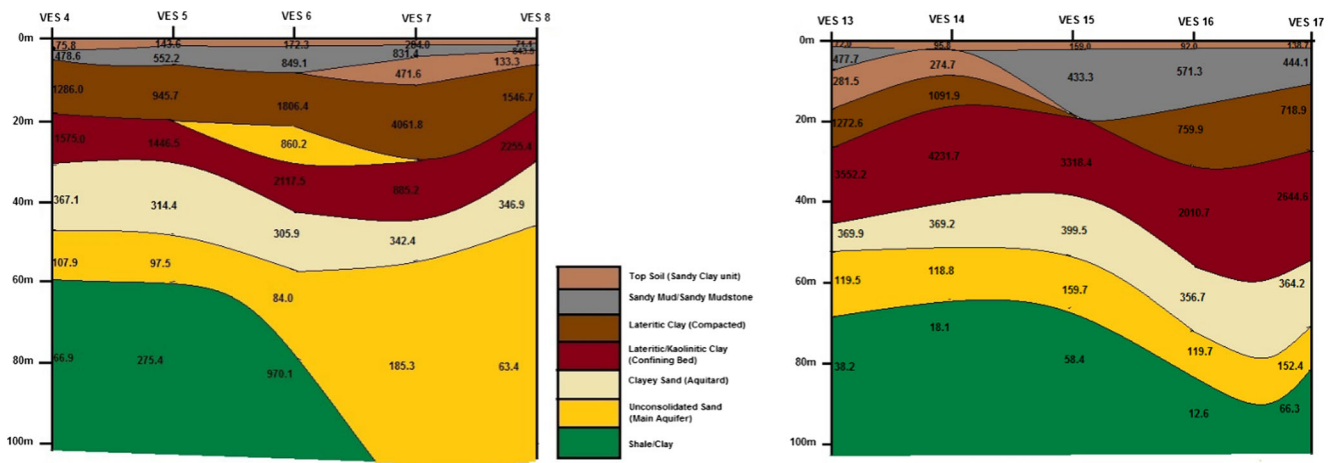
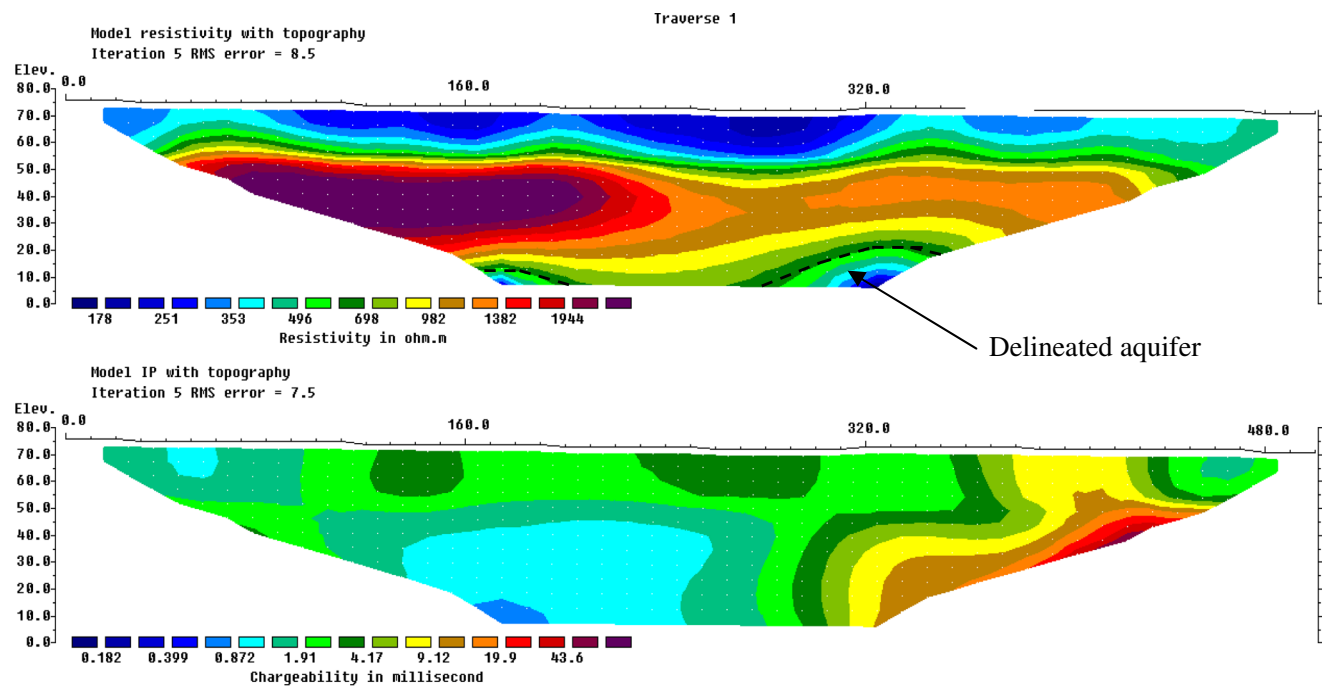


**Fig. 6** Representative geoelectric cross-sections constructed from the geoelectric parameters of the delineated layers for selected resistivity soundings

The sixth layer is equally a very resistive unit; it is relatively thick and laterally continuous across the study area. The model resistivity and thickness of this layer is largely uniform across the sounding curves. The high resistive unit is underlain by a relatively low resistive clayey sand unit with largely uniform model resistivity ranging from 278.7–415.3  $\Omega$ m and an appreciable thickness ranging from 10.1–16.2 m, respectively. Underlying the clayey sand is an unconsolidated sand unit characterized with low resistivity that ranges from 58.8–228.3  $\Omega$ m and a thickness that is largely uniform ranging between 11.8 and 13.3 m, except in VES 6 where the thickness delineated is 19.2 m; it is thought that the underlying unit

at this VES point could not be distinguished (no resistivity contrast) from this sand unit and this possibly accounts for the large thickness delineated. The last layer delineated is thought to be a clayey/shale unit due to its very low resistivity; however, this layer was not penetrated or distinguished from the overlying unit in some of the VES locations.

In general, the geoelectric layers delineated from the resistivity soundings (Table 1 and Fig. 6) are laterally continuous across the entire study area and correlate well in terms of geoelectric-lithology as expected in a sedimentary terrain. In particular, the thicknesses and resistivities of the layers in the deeper section are largely uniform across the study area.



Horizontal scale is 23.98 pixels per unit spacing  
 Vertical exaggeration in model section display = 0.99  
 First electrode is located at 0.0 m.  
 Last electrode is located at 500.0 m. Unit Electrode Spacing = 10.0 m.

**Fig. 7** 2D inverse model resistivity and chargeability for traverse 1

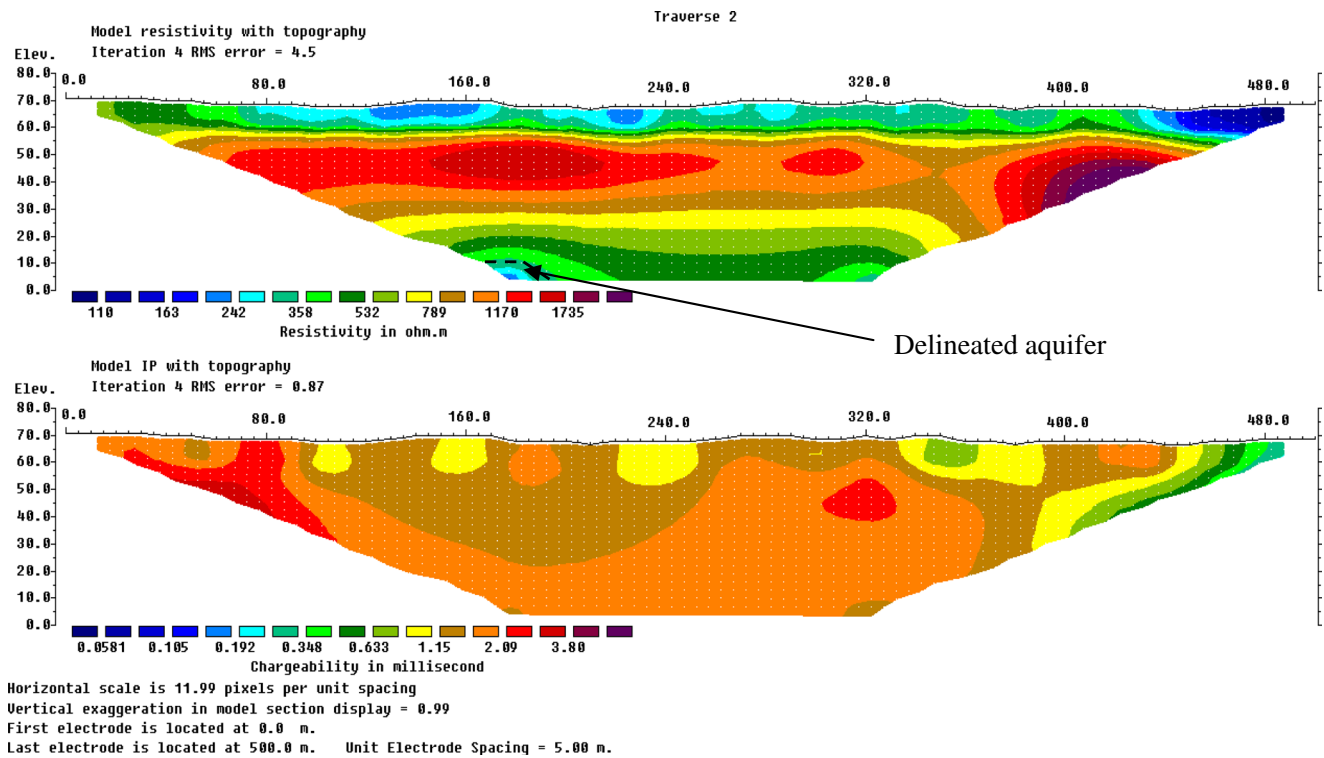


Fig. 8 2D inverse model resistivity and chargeability for traverse 2

Layers 3 and 5 are not observed in some of the VESs points and are thought to be sandy/silty clay and sand lenses, respectively. In particular, layer 5 may have been masked in some of the VESs locations due to the high resistivity values of layers

4 and 6; also, it may have thin-out completely in some cases as observed in VESs 1, 6, 11, 18, 22, and 23 locations. The observed clay and sand lenses together with large variations in the model resistivity of the upper section depict rapid lateral

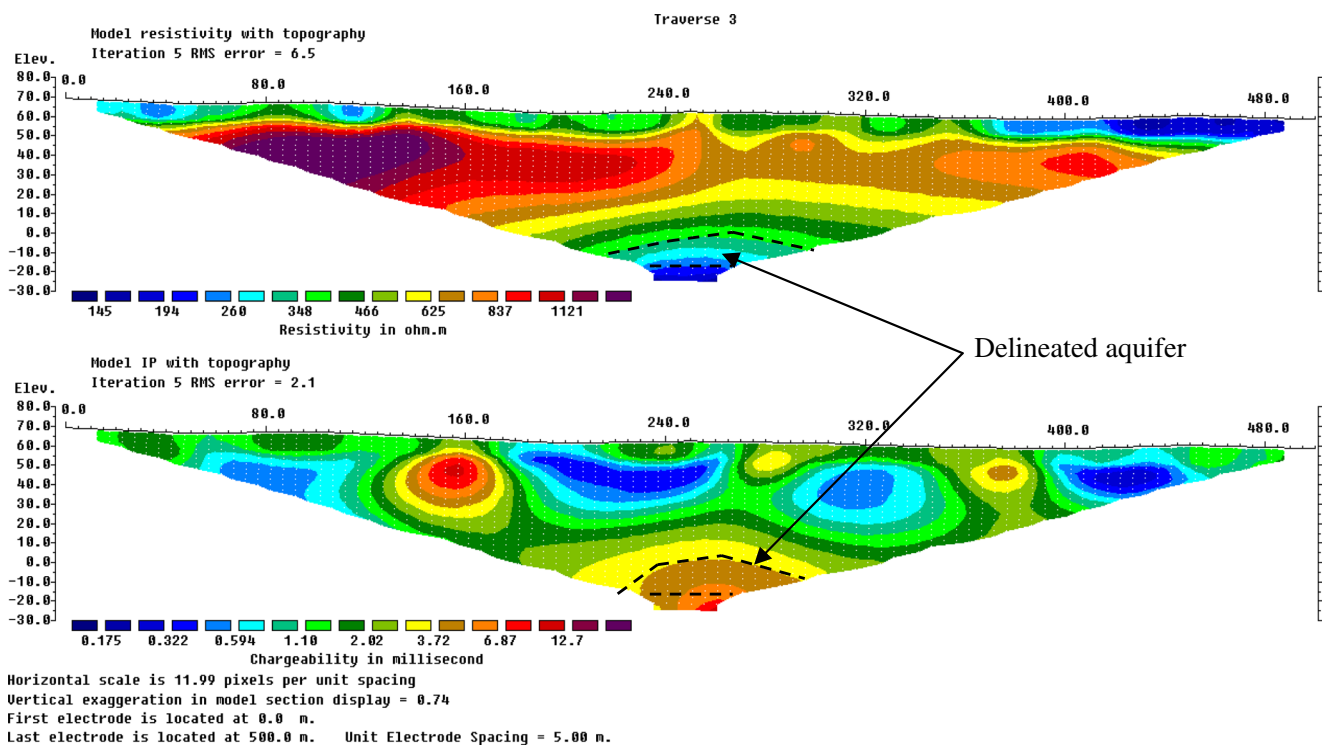
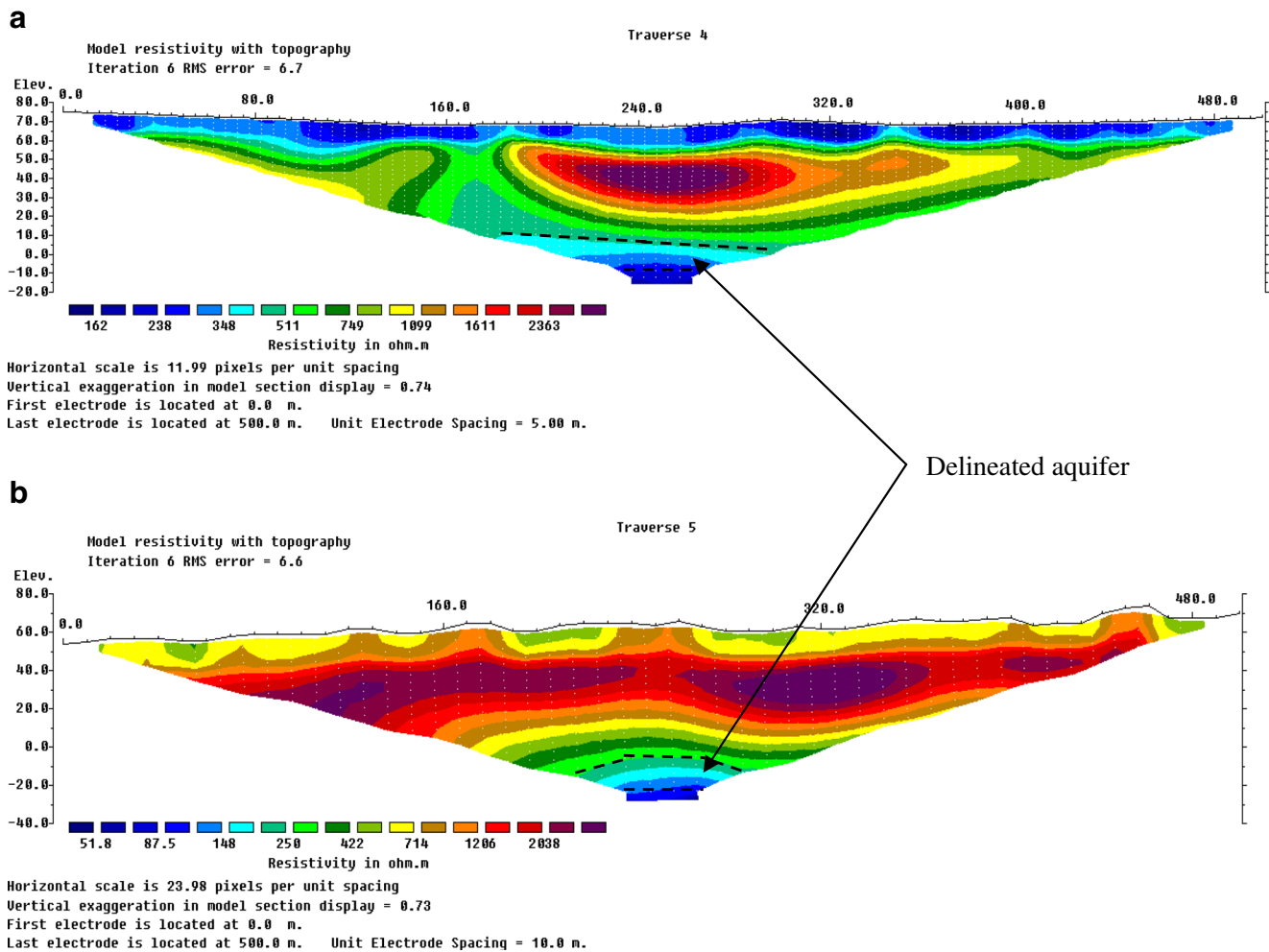


Fig. 9 2D inverse model resistivity and chargeability for traverse 3



**Fig. 10** 2D inverse model resistivity for: **a** traverse 4 and **b** traverse 5

facies changes and near-surface heterogeneities that commonly characterized the Ilaro Formation (Ogbe 1970; Okosun 1990). Samples from drilled and hand-dug wells indicate that the high resistive unit (layer 6 in Table 1 and Fig. 6) is highly consolidated and predominantly composed of swelling clay rich in kaolin and intercalated with phosphate minerals. The kaolin and phosphate minerals are thought to account for the high resistivity values observed for this relatively thick clayey unit.

The 2D model resistivity and chargeability images of the subsurface obtained from the inversion of the observed apparent resistivity and chargeability data are presented in Figs. 7, 8, 9, 10, 11 and 12). The inverse models of the 2D resistivity and chargeability images of the subsurface show a general geoelectric-lithology trend very similar to that observed in the resistivity soundings. Reasonable correlation exists between the 2D inverse models and the geoelectric layered parameters obtained from the soundings. The lateral continuities of geoelectric layers (geoelectric-lithology) and near-surface heterogeneity observed in the resistivity soundings are clearly depicted in the inverted 2D resistivity images. The top soil

delineated in the resistivity soundings is not distinctly observed in the 2D images due to its small thickness (0.5–2.3 m averaging 1.18 m) relative to the minimum electrode spacing of 10.0 m used for the 2D survey. Evidence of the clay and sand lenses delineated in the resistivity soundings is observed traverse 6 (Fig. 11), where a sand lens overlies a clay lens. The sand lenses often form shallow perched aquifers in the area which may not yield appreciable groundwater to drilled wells.

The unconsolidated sand unit in the geoelectric sounding parameters (layer 8 in Table 1 and Fig. 6), which is observed to be laterally continuous with relatively uniform model resistivity and thickness in the entire areal extent, is thought to be the main (regional) aquifer body in the area. The 2D inverse model resistivity of the delineated aquifer unit ranges from about 75–150  $\Omega$ m; this corresponds to the model resistivity observed in the resistivity soundings for the same geoelectric unit (layer 8 in Table 1 and Fig. 6). The main aquifer unit delineated in the 2D resistivity and chargeability images is well penetrated in traverses 3, 4, 5, and 7 (Figs. 9, 10, and 12) but partially penetrated in traverses 1, 2, and 6 (Figs. 7, 8,

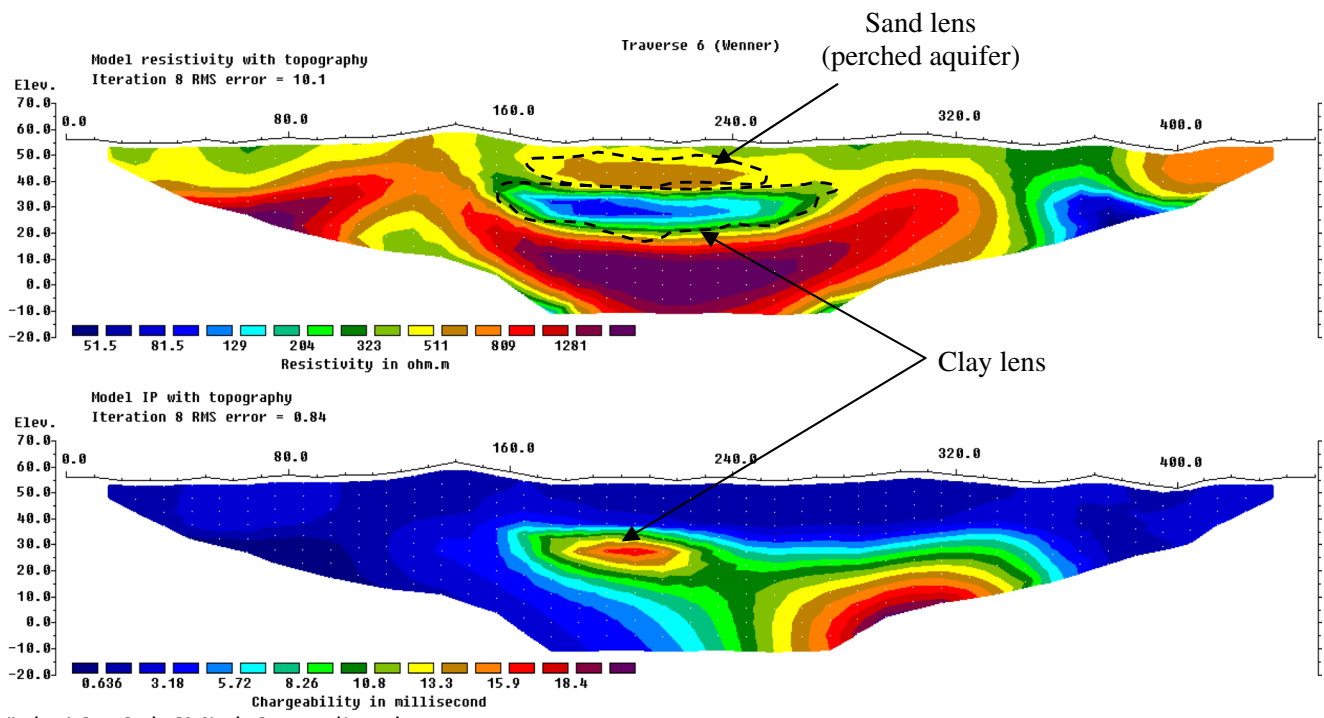


Fig. 11 2D inverse model resistivity and chargeability for traverse 6

and 11). This is due to the fact that data level of 12 (minimum electrode spacing of 10–120 m) was used for the data measurements in traverses 1, 2, and 6 as against data level of 16 (minimum electrode spacing of 10–160 m) used for the data

measurements of other traverses. The 2D resistivity images show that the delineated aquifer occurs at an elevation of about 5 m to about 20 m below mean sea level corresponding to an average depth-to-aquifer of about 80 to 100 m and

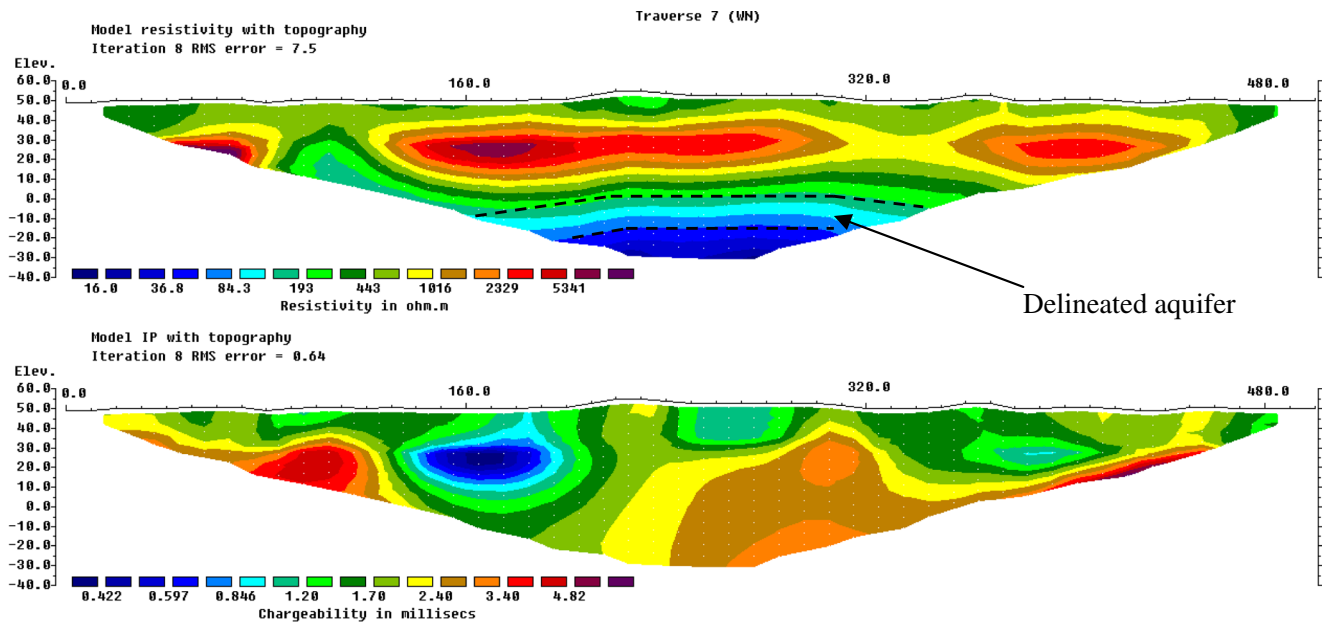


Fig. 12 2D inverse model resistivity and chargeability for traverse 7

average aquifer thickness of about 15 m. This model thickness agrees reasonably well with that observed in the geoelectric parameters of the resistivity soundings.

The main aquifer unit delineated is overlain by a relatively more resistive layer that is also observed to be laterally continuous in the entire area in both the 2D images and the resistivity soundings. The layer is characterized with relatively uniform inverse model resistivity value that range from about 280–400  $\Omega\text{m}$  and an average thickness of about 12.3 m. This unit is saturated but relatively impermeable; consequently, it serves both as a confining bed and aquitard to the main aquifer body. Most hand-dug wells in the area are tapping groundwater from this aquitard unit because of the large diameters with which the wells are dug.

The aquitard unit is overlain with a relatively thick and very resistive layer that is conspicuously observed in the 2D resistivity images of all the traverses as well as the resistivity soundings. This layer is laterally continuous across the entire area but the resistivity varies spatially due to changes in the degree of compaction and mineralogy. The chargeability anomaly (IP effect) observed for this high resistive layer is not very distinct, but a careful observation of the chargeability images show that the high resistive layer is characterized with a moderately high chargeability anomaly indicating massive or compacted clayey lithology for the layer. This is consistent with the results of previous studies conducted within the same geologic environment (Aizebeokhai and Oyeyemi 2014).

The aquifer unit is underlain by a very low resistivity unit as shown in both the 2D inverse models and the geoelectric parameters of the resistivity soundings (layer 9 in Table 1 and Fig. 6). This low resistivity unit is characterized with a distinct high chargeability anomaly as observed in traverses 3 and 7 (Figs. 10 and 12). The observed high chargeability anomaly for this low resistivity unit indicates that the delineated aquifer is underlain with clayey/shaley formation. This is also consistent with similar studies conducted around the area (Aizebeokhai and Oyebanjo 2013; Aizebeokhai and Oyeyemi 2014).

## Conclusion

Geophysical survey involving resistivity sounding and 2D resistivity and time-domain IP imaging was carried out in Iyana-Iyesi and Canaan Land area, southwestern Nigeria. The survey is part of a preliminary assessment of the groundwater resource potential in the area. The knowledge of groundwater resource potential is essential for groundwater resource development planning as well as groundwater resource management and monitoring. The near-surface was characterized by integrating the geoelectric layered parameters obtained from the resistivity soundings with the 2D resistivity and chargeability inversion models. This integration is

found to be effective in characterizing near-surface heterogeneities. The aquifer unit delineated is thought to be high-yield regional aquifer and is confined by a low yield aquitard. The thickness of the aquifer delineated is largely uniform and average of about 12.5 m; depth to the aquifer progressively increases northward in the basin.

**Acknowledgments** The authors wish to thank Covenant University Management for providing the resources to conduct this study. Our profound appreciation goes to following undergraduate students who helped with the field data collection: Nelson-Atuonwu Cherish, Liadi Esther, Shotuyo Yewade, Lesinwa Fortune, Ijioma Nanna, Utor Joy, Tucker Miata, Uye Perpetual, and Ukabam Chukwuemeka.

## References

- Amidu SA, Olayinka AI (2006) Environmental assessment of sewage disposal systems using 2D electrical resistivity imaging and geochemical analysis: a case study from Ibadan, southwestern Nigeria. *Environ Eng Geosci* 7(3):261–272
- Aizebeokhai AP, Alile OM, Kayode JS, Okonkwo FC (2010a) Geophysical investigation of some flood prone areas in Ota, southwestern Nigeria. *Am-Eurasian J Sci Res* 5(4):216–229
- Aizebeokhai AP, Olayinka AI, Singh VS (2010b) Application of 2D and 3D geoelectrical resistivity imaging for engineering site investigation in a crystalline basement terrain, southwestern Nigeria. *Environ Earth Sci* 61(7):1481–1492. doi:10.1007/s12665-010-0474-z
- Aizebeokhai AP, Oyebanjo OA (2013) Application of vertical electrical soundings to characterize aquifer potential in Ota, Southwestern Nigeria. *Int J Phys Sci* 8(46):2077–2085
- Aizebeokhai AP, Oyeyemi KD (2014) The use of multiple-gradient array for geoelectrical resistivity and induced polarization imaging. *J Appl Geophys* 111:364–376. doi:10.1016/j.jappgeo.2014.10.023
- Billman HG (1992) Offshore stratigraphy and paleontology of Dahomey (Benin) embayment. *NAPE Bull* 70(2):121–130
- Chambers JE, Kuras O, Meldrum PI, Ogilvy RD, Hollands J (2006) Electrical resistivity tomography applied to geologic, hydrogeologic and engineering investigations at a former waste-disposal site. *Geophysics* 71(6):B231–B239
- Chambers JE, Wilkinson PB, Kuras O, Ford JR, Gunn DA, Meldrum PI, Pennington CVI, Weller AI, Hobbs PRN, Ogilvy RD (2011) Three-dimensional geophysical anatomy of an active landslide in Lias group mudrocks, Cleveland Basin, UK. *Geomorphology* 125(4):472–484
- Chandra S, Ahmed A, Ram A, Dewandel B (2008) Estimation of hard rock aquifers hydraulic conductivity from geoelectrical measurements: a theoretical development with field application. *J Hydrol* 357:218–227. doi:10.1016/j.jhydrol.2008.05.023
- Dahlin T, Bernstone C, Loke MH (2002) A 3D resistivity investigation of a contaminated site at Iernacken in Sweden. *Geophysics* 60(6):1682–1690
- Dahlin T, Loke MH (1998) Resolution of 2D Wenner resistivity imaging as assessed by numerical modelling. *J Appl Geophys* 38(4):237–248
- Day-Lewis FD, Singha K, Binley AM (2005) Applying petrophysical models to radar travel time and electrical resistivity tomograms: resolution-dependent limitations. *J Geophys Res Solid Earth* 110: B08206. doi:10.1029/2004JB003569
- Gebhardt H, Adekeye OA, Akande SO (2010) Late Paleocene to initial Eocene thermal maximum foraminifera biostratigraphy and paleoecology of the Dahomey Basin, southwestern Nigeria. *Gjahrung Der Geologischchem Bundesantalt* 150:407–419

- Griffiths DH, Barker RD (1993) Two dimensional resistivity imaging and modelling in areas of complex geology. *J Appl Geophys* 29:211–226
- Hubbard SS, Chen J, Peterson JE, Mayer EL, Williams KH, Swift DJ, Mailloux B, Rubin Y (2001) Hydrogeological characterisation of the south oyster bacterial transport site using geophysical data. *Water Resour Res* 37(10):2431–2456
- Hubbard SS, Rubin Y, Majer EL (1999) Spatial correlation structure estimation using geophysical and hydrogeological data. *Water Resour Res* 35(6):2659–2670
- Loke MH, Barker RD (1996) Practical techniques for 3D resistivity surveys and data inversion. *Geophys Prospect* 44:499–524
- Loke MH, Chambers JE, Rucker DF, Kuras O, Wilkinson PB (2013) Recent developments in the direct-current geoelectrical imaging method. *J Appl Geophys* 95:135–156
- Massoud U, Santos FM, Khalil MA, Taha A, Abbas MA (2010) Estimation of aquifer hydraulic parameters from surface geophysical measurements: a case study of the upper cretaceous aquifer, Central Sinai, Egypt. *Hydrogeol J* 18:699–710. doi: [10.1007/s10040-009-0551-y](https://doi.org/10.1007/s10040-009-0551-y)
- Niwas S, Celik M (2012) Equation estimation of porosity and hydraulic conductivity of Ruhrtal aquifer in Germany using near surface geophysics. *J Appl Geophys* 84:77–85
- Obaje NG (2009) Geology and mineral resources of Nigeria. In: Brooklyn SB, Bonn HJN, Gottingen JR, Graz KS, (ed), *Lecture Notes in Earth Sciences*, Springer, 120:22
- Ogbe FAG (1970) Stratigraphy of strata exposed in the Ewekoro quarry, western Nigeria. In: Dessauvage TFJ, Whiteman AJ (eds) *African geology*. University of Ibadan Press, Nigeria, pp. 305–324
- Okosun EA (1990) A review of the cretaceous stratigraphy of the Dahomey embayment, West Africa. *Cretac Res* 11:17–27
- Olabode SO (2006) Siliciclastic slope deposits from the cretaceous Abeokuta group, Dahomey (Benin) basin, southwestern Nigeria. *J Afr Earth Sci* 46:187–200
- Omatsola ME, Adegoke OS (1981) Tectonic evolution and cretaceous stratigraphy of the Dahomey Basin. *Nigerian J Min Geol* 18(1): 130–137
- Onuoha KO (1999) Structural features of Nigeria's coastal margin: an assessment based on age data from wells. *J Afr Earth Sci* 29(3): 485–499
- Rubin Y, Hubbard S (2005) *Hydrogeophysics, water science and technology library 50*. Springer, Berlin, p. 523
- Rucker D, Loke MH, Levith MT, Noonan GE (2010) Electrical resistivity characterization of an industrial site using long electrodes. *Geophysics* 75(4):WA95–WA104
- Vereecken H, Binley A, Cassiani G, Kharkhordin I, Revil A, Titov K (eds) (2006) *Applied Hydrogeophysics*, Springer-Verlag, Berlin, 372
- Wilson SR, Ingham M, McConchie JA (2006) The applicability of earth resistivity methods for saline interface definition. *J Hydrol* 316(1–4):301–312
- Wilson RCC, Williams CA (1979) Oceanic transform structures and the developments of Atlantic continental margin sedimentary basin: a review. *J Geol Soc Lond* 136:311–320